Decentralized Dispatch of Distributed Multi-Energy Systems with Comprehensive Regulation of Heat Transport in District Heating Networks

Qinghan Sun, *Student Member, IEEE*, Tian Zhao, Qun Chen, *Member, IEEE*, Kelun He, and Huan Ma

***Abstract*—Distributed Energy Systems(DES) interconnected with Electric Power Network(EPN) and District Heating Network(DHN) have drawn great attention recently as they promote user-side coordination of multi-energy flows. However, the difference of physical nature between electric power transmission and heat transport has brought difficulties to the modelling and decentralized optimization. In this work, a new DHN model considering delay and storage features of pipeline heat migration and heat transfer between fluids is proposed through trigonometric expansion of the decision series and the heat current method. The model comprehensively characterizes the heat transport in the system and a dispatch problem considering hybrid regulation of fluid flow rates and temperatures in DHN is then established. A primal-decomposition-based decentralized gradient descent method in accompany with Alternating Direction Method of Multipliers(ADMM) is proposed to optimize the DESs in a fully decentralized manner. Case study on two test systems validates the effectiveness of the proposed model and method to further harness the potential of DHN, which reduces renewable energy curtailment by 17.3% and 27.0% respectively.**

***Index Terms*—Distributed Energy Systems, District Heating Networks, Decentralized Optimization, Renewable Energy Sources, Alternating Direction Method of Multipliers**

I. Introduction

DISTRIBUTED Energy System(DES) is a promising solution to accomplish carbon neutrality, which consists of multi-energy sources, e.g., distributed renewables, fossil-fuel-based cogenerators and energy conversion and storage devices to meet end-users' diverse demands [1]. Meanwhile, with the Electric Power Network(EPN), the interconnected DESs are more resilient to demand and renewable energy fluctuations and thus have the potential to behave collaboratively. Besides, the District Heating Network(DHN) with delay and storage characteristics temporally decouples the heat generations and loads and thus can provide more flexibility to the renewable sources. Structurally, the DESs, usually belonging to different agents, also reveal a decentralized nature. Therefore, a decentralized coordination scheme may be preferred compared to the centralized dispatch through a system operator. The decentralized scheme encourages each DES agent to share information with neighbours and participate in the dispatch directly, which protects privacy, enables parallel calculation and improves solution robustness in case of single-point failure [2].

Nevertheless, the difference of physical nature between multi-energy flows has brought difficulties to the modelling and optimization of networked DESs. In general, the DHN is composed of a primary heating network(PHN) and multiple secondary networks(SHN). The SHNs separate end users from the high pressure high temperature PHN to ensure safety and heating comfort. Therefore, the heat transport in DHN consists of both heat migration accompanying with fluid flow and heat transfer between fluids with different temperatures, which are obviously different from EPN.

From the modelling perspective, extensive efforts have been made to concise mathematical descriptions of the DHN. A straightforward approach is to derive a group of partial differential equations based on energy conservation [3]–[5]. Although the equations accurately reflect pipeline delay and losses and can be solved through finite difference methods, solving them in optimization problems can be difficult. Therefore, simplifications are made and some attempts [6]–[11] simulating or optimizing integrated power and heating systems may dismiss the pipeline delay or losses. In [12], a node method is proposed to capture the quasi-dynamics of temperatures, which represents pipeline outlet temperatures as the weighted average temperature of several historical time sections at the inlet. The node method can be seen as using the upwind scheme to discretize the differential equations at each dispatch period, and the numerical diffusion of temperature waves [13], [14] may occur when the pipeline delay time is not an integer multiple of the dispatch interval. Another approach to the differential equations is to switch to the frequency domain. In [15], Chen et al. propose a general phasor method, which uses Fourier transform to reformulate mass-constant heat flow constraints into phasor forms and reduces calculation errors. In [16], Laplace transformation is used to derive an "end-to-end" temperature relationship between heat generation and demand. It is worth noting that [15] and [16] are based on the assumption that fluid flow rates remain constants.

The above methods mainly concern the heat migration through pipeline flows in the PHN, and the heat transfer constraints considering the heat transfer ability of the SHN are ignored casually. Indeed, as users' room temperature and operation status of local devices in the DESs vary in a day,

This work was supported by the National Natural Science Foundation of China under Grant 51836004 and Grant 52125604. (Corresponding author: Qun Chen.)

Qinghan Sun, Tian Zhao, Kelun He and Huan Ma are with the Department of Engineering Mechanics, Tsinghua University, Beijing 100084, China (e-mail: sqh20@mails.tsinghua.edu.cn, zhaotian@tsinghua.edu.cn, hekl@mail.tsinghua.edu.cn, mh17@mails.tsinghua.edu.cn)

Qun Chen is with the Department of Engineering Mechanics, and the Department of Electrical Engineering, Tsinghua University, Beijing 100084, China (e-mail: chenqun@tsinghua.edu.cn)

different PHN flow temperatures are requested by different DESs at different periods. The heat transfer constraints are important if users' heating comfort are to be ensured in the dispatch. To model this, [17] uses the heat resistance to constrain the heat transfer from the PHN to end users without considering various distributed energy conversion devices and flexible SHN adjustment. In [18], a heat current model is proposed for heat transfer systems and applied in integrated analysis with the EPN. [19] further extend the heat current method to model both heat migration and transfer in the DHN. This method embeds nonlinearity into nonlinear circuit elements and linear circuits, enabling a timing simulation of integrated power and heating systems. Despite the current lack of practice, the heat transport throughout DHN with various DESs can be modelled comprehensively through a combination of the reviewed researches.

Based on these modelling methods, researchers have designed various centralized or decentralized dispatch techniques considering different DHN regulation schemes. The quality-regulation mode which adjusts flow temperatures and treats flow rates as given constants is widely applied in practical PHNs due to stable hydraulic conditions [20]. Therefore, many researches [17], [21]–[25] follow this practice to optimize the integrated power and heating system. Among them, the node-method-based modelling has been most popular as the weights can be easily calculated with given fluid flow rates and the model is linear and tractable in terms of temperatures. Besides, the frequency-domain-based methods and the heat current methods are also linear and applicable when fluid flow rates are given constants. However, the adjustment of fluid flow rates in the PHN, i.e., quantity regulation, is promising in economy as their effects permeate the entire system with respect to delay time, heat capacities and thermal resistances at the heat exchange stations. Therefore, the quality regulation alone cannot fully reflect and exploit the storage potential of heat transport in DHN. When the decisions of those fluid flow rates are involved, all of the DHN modelling methods can exhibit very strong nonlinear properties if delay characteristics are to be included. For example, in the node method, the weights are non-smooth functions of fluid flow rates and thus gradient-based numerical optimization is not applicable. Possible optimization solutions considering quantity regulation and delay characteristics include fixed-point iterations [26], [27] and heuristic techniques such as the genetic method [5]. Notwithstanding, the discontinuous mapping relationship of the fixed-point method and the randomness consequent upon the heuristic algorithms create an obstacle for the design of an effective decentralized optimization process on the user side.

So far, few researchers have yet modelled the heat migration and transfer in DHN thoroughly considering complementary heating techniques among DESs and analyzed how can the overall heat transport be rationally regulated through a co-optimization of fluid flow rates and temperatures in DHN under decentralized schemes. To fill the gaps, this work aims to present a synthetic model of the DHN and propose a fully decentralized optimization method for connected multi-energy DESs which mainly adopts temperature regulation in PHN, while a daily adjustment of fluid flow rates considering delays is also considered. The main contributions are as follows:

1) A new DHN model following the basic idea of frequency domain analysis, i.e., applying Fourier Transform or trigonometric expansion to nodal temperatures, is established to model pipeline delay and losses considering the daily variation of fluid flow rates. Besides, the heat transfer constraints between fluids of different temperatures are also considered through the heat current method. On this basis, an optimization model is established where the heat transport between interconnected DESs is comprehensively characterized.
2) To deal with the non-convexity caused by modelling fluid flow rates adjustment, a primal-decomposition-based gradient descent method in company with the Alternating Direction Method of Multipliers(ADMM) is proposed to optimize distributed multi-energy systems considering temperature and daily flow rates regulation in a fully decentralized manner.
3) Case study on two integrated systems validates the effectiveness of the proposed method compared with two baseline methods. The proposed method reduces the curtailment rate of renewable energy by 17.3% and 27.0% respectively compared to the case without fluid flow rate regulation. The total operation cost is also reduced by 5.4% and 6.8% respectively.

This article is an extension of our previous conference paper [28]. The initial conference paper combines the node method and heat current method to model the heat transport in DHN and uses ADMM to do agent-based fully decentralized dispatch, while fluid flow rates in the DHN are preset parameters. This work enables daily fluid flow rate regulation and provides more insight into the significance of comprehensive modelling and regulation of heat transport. The remainder of this article is organized as follows: Section II describes the distributed multi-energy systems with EPN and DHN. Section III proposes the fully decentralized solution. Section IV presents the case study.

II. Mathematical model of networked DESs

A. System Structure and Regulation Framework

Fig. 1(a) reveals the general structure of a DES to be studied, which is implemented with micro-turbine-based combined heat and power(CHP) systems, heat pumps(HP) and renewable sources such as photovoltaic(PV) panels and wind turbines(WT). These multi-energy sources and energy converters work together to meet the demands of shopping malls, hospitals or industrial facilities. The DES can exchange power with the EPN to maintain power balance. Besides, the heating devices in the system are connected through a secondary heating network(SHN), which exchange heat with the primary heating network(PHN) through a heat exchange station(HES). The SHN and PHN constitute the self-sufficient DHN. The DESs can either work in heat source(HS) or heat customer(HC) modes. In the HC mode(Fig. 1(a)), local devices and the PHN work together to meet the heat demand of end-users. In the HS mode(Fig. 1(b)), the fluid flow direction in SHN is different and the DES will work reversely as a heat source of the PHN. Fig. 1.(c) shows the structure of networked

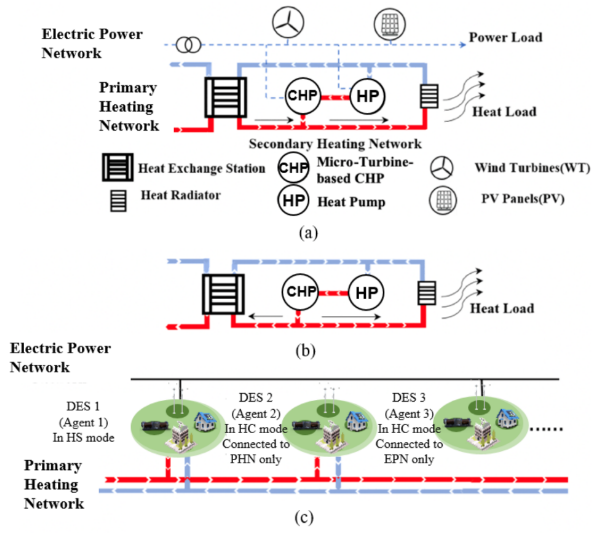

Fig. 1. The general structure of networked DESs: (a) DES in the HC mode. (b) DES in the HS mode, the flow directions are different from (a). (c) Multiple DESs connected with the PHN and EPN.

DESs connected through the EPN and PHN. The DESs can connect to one or both of the networks.

As can be seen from Fig. 1, the PHN and SHN may have quite different spatial sizes. The SHNs reveal the topology of local energy sources and belong to specific DESs. Contrariwise, the PHN connects multiple SHNs, i.e., multiple DESs, on a larger scale. Due to safety reasons and engineering practices, we consider an interday quantity regulation and intraday quality regulation scheme of the PHN. The quantity regulation of flow rates is executed at the beginning of every day, while quality regulation of flow temperatures is performed hourly or every 15 minutes. As for the SHN, the flow rates of fluids that enter the HES and the fluid temperatures can be flexibly adjusted at all times under operational constraints. A day-ahead dispatch based on both historical DHN operation status and demand and renewable energy predictions is considered.

B. Modelling of PHN

The PHN includes symmetric supply and return pipelines and HESs to exchange heat with the DESs. We consider a radial PHN.

1) Pipelines: We first consider a constant fluid flow rate $\dot{m}$ in the PHN pipelines and neglect the heat conduction between fluid microelements, the inlet and outlet temperatures have the following relationship [29].

$$\theta_{out}(t) = \theta_{in}(t - t_d)e^{-\frac{UL}{\dot{m}c_p}} \tag{1}$$

where $\theta_{out}(t) = T_{out}(t) - T_a$ and $\theta_{in}(t) = T_{in}(t) - T_a$ are the excess temperatures at the pipeline inlet and the outlet. T_a is the ambient temperature. U is the heat transfer coefficient between the fluid and the surrounding environment. L denotes the pipeline length. ρ and c_p are the density and the heat capacity of the fluid. $t_d = \frac{\rho AL}{\dot{m}}$ is the delay time, where A is the pipeline cross section area.

Since optimization can only be performed on discrete time slots, (1) should be discretized based on the dispatch time intervals, Δt. Noting that the time delay t_d may not be an integer multiple of Δt, interpolation of temperature decisions adjacent in time may lead to a non-smooth structure in terms of $\dot{m}$. To deal with this problem, we follow the idea of frequency-domain analysis [15], [16], and apply Discrete Fourier Transform(DFT) to discrete temperatures to obtain phasor forms. For a better illustration, we demonstrate DFT in the form of trigonometric series on the real number field:

$$\theta[i] \triangleq \theta(i\Delta t) = \sum_{k=0}^{\frac{M}{2}} \widetilde{\theta}[k]\cos k\omega i + \sum_{k=1}^{\frac{M}{2}-1} \widetilde{\theta}[k+\frac{M}{2}]\sin k\omega i \tag{2}$$

where $\theta[i]$ is the discrete decision variables of pipeline node temperatures. M denotes the length of θ and is assumed to be even-numbered. $\tilde{\theta}$ is the coefficient of the trigonometric series, and can also be treated as decisions in the frequency domain. $\omega = 2\pi/M$ is the base frequency. The matrix form of (2) is:

$$\theta = \mathbf{A}\widetilde{\theta} \tag{3}$$

$$\mathbf{A}_{ij} = \begin{cases} \cos\omega ij & j = 0, ..., \frac{M}{2} \\ \sin\omega i\left(j - \frac{M}{2}\right) & j = \frac{M}{2}+1, ..., M-1 \end{cases} \quad i = 0, ..., M-1 \tag{4}$$

wheret ij denotes the ith row and jth column of a matrix.

$\tilde{\theta}$ can be used to estimate $\theta_{out}(t)$ for arbitrary t. Substitute $\theta_{out}(\cdot)$ and $\theta_{in}(\cdot)$ in (1) with their trigonometric-series-based approximations and discretize it on the dispatch periods, and we obtain,

$$\begin{aligned} \theta_{out}[i] &= \sum_{k=0}^{\frac{M}{2}} \widetilde{\theta}_{out}[k]\cos k\omega i + \sum_{k=1}^{\frac{M}{2}-1} \widetilde{\theta}_{out}[k+\frac{M}{2}]\sin k\omega i \\ &= \theta_{out}(i\Delta t) = \theta_{in}(i\Delta t - t_d)e^{-\frac{UL}{\dot{m}c_p}} \\ &= \left(\sum_{k=0}^{\frac{M}{2}} \widetilde{\theta}_{in}[k]\cos k\omega\left(i - \frac{t_d}{\Delta t}\right)\right. \\ &\left. + \sum_{k=1}^{\frac{M}{2}-1} \widetilde{\theta}_{in}[k+\frac{M}{2}]\sin k\omega\left(i - \frac{t_d}{\Delta t}\right)\right) e^{-\frac{UL}{\dot{m}c_p}} \end{aligned} \tag{5}$$

The matrix form of (5) is presented as:

$$\theta_{out} = \mathbf{A}\widetilde{\theta}_{out} = \mathbf{AB}\widetilde{\theta}_{in} = \mathbf{ABA}^{-1}\theta_{in} \tag{6}$$

where $\mathbf{B}$ is a $\dot{m}$-dependent matrix indicating delay and loss characteristics

$$\begin{aligned} \mathbf{B} &= e^{-\frac{UL}{\dot{m}c_p}} \begin{bmatrix} 1 & 0 & 0 & 0 \\ 0 & \mathbf{B}_{\cos} & 0 & -\mathbf{B}_{\sin} \\ 0 & 0 & \cos\frac{Mt_d\omega}{2\Delta t} & 0 \\ 0 & \mathbf{B}_{\sin} & 0 & \mathbf{B}_{\cos} \end{bmatrix} \\ \mathbf{B}_{\cos} &= diag\left(\cos\frac{t_d\omega}{\Delta t}, \cos\frac{2t_d\omega}{\Delta t}, ..., \cos\frac{\left(\frac{M}{2}-1\right)t_d\omega}{\Delta t}\right) \\ \mathbf{B}_{\sin} &= diag\left(\sin\frac{t_d\omega}{\Delta t}, \sin\frac{2t_d\omega}{\Delta t}, ..., \sin\frac{\left(\frac{M}{2}-1\right)t_d\omega}{\Delta t}\right) \end{aligned} \tag{7}$$

The above deduction is based on the premise that fluid flow rates remain constants and that the temperature decisions are periodically executed. However, this is impractical and the history temperature series with possible different fluid flow rates should be modelled. Since fluid flow rates are regulated

every day, we can safely assume that the flow microelements entering every pipeline will encounter velocity variation once at most before the outlet. In other words, there are no "super-long" pipelines with delay time larger than 24 hours. In this case, the fluid microelement that encounter flow rate variations can be considered as successively passing two pipelines at different velocities. Bearing this in mind, we further assume that the flow direction remains unchanged. Without loss of generality, we stipulate that the fluid flow rates are regulated at $t = 0$ and dispatch decisions are made for $t \geq 0$. Then the analytic solution (1) has the following form:

$$\theta_{out}(t) = \begin{cases} \theta_{in}(t - t_d)\, e^{-\frac{UL}{\dot{m}c_p}} & t \geq t_d \\ \theta_{in}^{his}\left(\frac{\dot{m}}{\dot{m}^{his}}(t - t_d)\right) e^{-\frac{UL}{\dot{m}c_p} + a(t - t_d)} & t \leq t_d \end{cases}$$
$$a = \frac{-U}{\rho A c_p}\left(1 - \frac{\dot{m}}{\dot{m}^{his}}\right) \tag{8}$$

where θ_{in}^{his} and $\dot{m}^{his}$ represent historical inlet temperature and fluid flow rates for $t \leq 0$.

Define an auxiliary function θ_{in}^{ext} as the extended inlet temperature:

$$\theta_{in}^{ext}(t) = \begin{cases} \theta_{in}^{his}\left(\frac{\dot{m}}{\dot{m}_{his}}t\right) e^{at} & t \leq 0 \\ \theta_{in}(t) & t \geq 0 \end{cases} \tag{9}$$

It is obvious that,

$$\theta_{out}(t) = \theta_{in}^{ext}(t - t_d)\, e^{-\frac{UL}{\dot{m}c_p}} \tag{10}$$

Let $\Theta_{in}^{his}[i] = \theta_{in}^{his}(i\Delta t)$ with $i \in \{-M, ..., -1\}$ be the discrete sampling of historical temperature data $\theta_{in}^{his}(t)$, and $\Theta_{in}^{ext}[i] = \theta_{in}^{ext}(i\Delta t)$ with $i \in \{-M, ..., -1, 0, ..., M-1\}$ be the sampling of the extended inlet temperature function. Combining (2) and (9), it can be obtained that

$$\begin{aligned} \Theta_{in}^{ext}[i] &= \sum_{k=0}^{\frac{M}{2}} \widetilde{\Theta}_{in}^{ext}[k] \cos k\omega i + \sum_{k=1}^{\frac{M}{2}-1} \widetilde{\Theta}_{in}^{ext}[k + \frac{M}{2}] \sin k\omega i \\ &= \theta_{in}^{ext}(i\Delta t) = \theta_{in}^{his}\left(\frac{\dot{m}}{\dot{m}_{his}} i\Delta t\right) e^{ai\Delta t} \\ &= \left(\sum_{k=0}^{\frac{M}{2}} \widetilde{\Theta}_{in}^{his}[k] \cos k\omega \left(\frac{\dot{m}}{\dot{m}_{his}} i\right) \right. \\ &\quad \left. + \sum_{k=1}^{\frac{M}{2}-1} \widetilde{\Theta}_{in}^{his}[k + \frac{M}{2}] \sin k\omega \left(\frac{\dot{m}}{\dot{m}_{his}} i\right) \right) e^{ai\Delta t} \\ &\quad \text{when } i \in \{-M, ..., -1\} \end{aligned} \tag{11}$$

and that,

$$\begin{aligned} \Theta_{in}^{ext}[i] &= \Theta_{in}[i] \\ &\text{when } i \in \{0, ..., M-1\} \end{aligned} \tag{12}$$

Therefore, we have the following matrix form of (11) and (12):

$$\Theta_{in}^{ext} = \begin{bmatrix} \mathbf{L}_s \mathbf{L}_d \widetilde{\Theta}_{in}^{his} \\ \Theta_{in} \end{bmatrix} = \begin{bmatrix} \mathbf{L}_s \mathbf{L}_d \left(\mathbf{A}^{his}\right)^{-1} \Theta_{in}^{his} \\ \Theta_{in} \end{bmatrix} \tag{13}$$

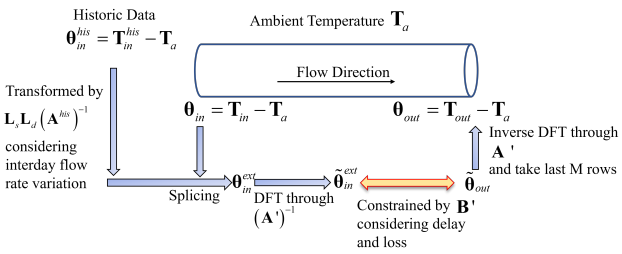

Fig. 2. The graphic explanation of (15)

where,

$$\begin{aligned} \mathbf{L}_s &= diag\left(e^{(-M)a\Delta t}, e^{(-M+1)a\Delta t}, ..., e^{(-1)a\Delta t}\right) \\ \mathbf{L}_{d,ij} &= \begin{cases} \cos\frac{\dot{m}}{\dot{m}^{his}}\omega(i - M)\, j & j = 0, ..., \frac{M}{2} \\ \sin\frac{\dot{m}}{\dot{m}^{his}}\omega(i - M)\left(j - \frac{M}{2}\right) & \\ \qquad\qquad j = \frac{M}{2} + 1, ..., M - 1 & \end{cases} \\ &\quad i = 0, ..., M - 1 \\ \mathbf{A}_{ij}^{his} &= \begin{cases} \cos\omega(i - M)j & j = 0, ..., \frac{M}{2} \\ \sin\omega(i - M)\left(j - \frac{M}{2}\right) & j = \frac{M}{2} + 1, ..., M - 1 \end{cases} \\ &\quad i = 0, ..., M - 1 \end{aligned} \tag{14}$$

Repeat the process of trigonometric interpolation in (5), we can obtain a matrix form similar to (6):

$$\Theta_{out} = \begin{bmatrix} \mathbf{0}_M \\ \mathbf{I}_M \end{bmatrix}^T \mathbf{A}'\mathbf{B}'\mathbf{A}'^{-1}\Theta_{in}^{ext} \tag{15}$$

The definition of $\mathbf{A}', \mathbf{B}' \in \mathbb{R}^{(2M)\times(2M)}$ above is similar to those in (4) and (7) except that they are defined for different discrete series and thus have different dimensions. It is worth noting that the converting matrix $\mathbf{A}'\mathbf{B}'\mathbf{A}'^{-1}$ is pre-multiplied by an extra $[\mathbf{0}_M \ \ \mathbf{I}_M] \in \mathbb{R}^{(M)\times(2M)}$ to take the last M rows. This is because we are only concerned about the decisions for $t \geq 0$, i.e., $i \in \{0, ..., M-1\}$.

A graphic explanation of (15) is also provided in Fig. 2. From (15) and Fig. 2, we can obtain an intuitive understanding of the pipeline dynamics considering quantity regulation. The historical flow temperature curve is first reshaped through the scaling matrix $\mathbf{L}_s$ and the dilation matrix $\mathbf{L}_d$ to include the impact of flow rate variation. The transformed historical curve and the pending decisions for the current period Θ_{in} are then spliced and delay and losses are considered through $\mathbf{B}'$.

If we partition $\mathbf{A}'\mathbf{B}'\mathbf{A}'^{-1}$ into block forms:

$$\mathbf{A}'\mathbf{B}'\mathbf{A}'^{-1} = \begin{bmatrix} \mathbf{K}_{M\times M}^{11} & \mathbf{K}_{M\times M}^{12} \\ \mathbf{K}_{M\times M}^{21} & \mathbf{K}_{M\times M}^{22} \end{bmatrix} \tag{16}$$

(15) can be further reduced to:

$$\Theta_{out} = \mathbf{K}_{M\times M}^{21}\mathbf{L}_s\mathbf{L}_d\left(\mathbf{A}^{his}\right)^{-1}\Theta_{in}^{his} + \mathbf{K}_{M\times M}^{22}\Theta_{in} \tag{17}$$

In other words,

$$\Theta_{ij,out} = \mathbf{C}_{ij,his}(\dot{m}_{ij})\,\Theta_{ij,in}^{his} + \mathbf{C}_{ij,cur}(\dot{m}_{ij})\,\Theta_{ij,in} \tag{18}$$

Herein, we abuse the notations of i, j and ij to label the DHN nodes and pipelines instead of representing terms in a matrix(c.f. (4)). ij indicates the flow direction from DHN node i to j. $\mathbf{C}_{ij,his}(\cdot) = \mathbf{K}_{M\times M}^{21}\mathbf{L}_s\mathbf{L}_d\left(\mathbf{A}^{his}\right)^{-1}$ and $\mathbf{C}_{ij,cur}(\cdot) = \mathbf{K}_{M\times M}^{22}$ are differentiable matrix functions of flow rate $\dot{m}_{ij}$, which enable the gradient-based optimization approach.

Noting that the pipelines also exhibit storage capabilities, a periodic boundary condition should be imposed:

$$\begin{aligned}\int_{t=0}^{t_{end}} \frac{\mathrm{d}H_{sto}}{\mathrm{d}t}dt &= \int_{t=0}^{t_{end}} (\Phi_{ij,in} - \Phi_{ij,out} - \Phi_{ij,loss})dt \\ &\approx \int_{t=0}^{t_{end}} \dot{m}c_p \left(\theta_{ij,in} e^{-\frac{U_{ij}L_{ij}}{\dot{m}_{ij}c_p}} - \theta_{ij,out}\right)dt = 0\end{aligned} \tag{19}$$

The discrete form of constraint (19) is given as:

$$e^{-\frac{U_{ij}L_{ij}}{\dot{m}_{ij}c_p}} \mathbf{1}^{\mathrm{T}}\boldsymbol{\theta}_{in} = \mathbf{1}^{\mathrm{T}}\boldsymbol{\theta}_{out} \tag{20}$$

2) Pipeline junctions: At the junction i of the pipelines, the conservation of fluid flow rates gives the following constraints:

$$\sum_{j\to i} \dot{m}^s_{ji} = \sum_{i\to k} \dot{m}^s_{ik} + \dot{m}_i \tag{21}$$

$$\sum_{i\to j} \dot{m}^r_{ij} = \sum_{k\to i} \dot{m}^r_{ki} + \dot{m}_i \tag{22}$$

where s and r discriminate between the symmetric supply and return pipelines and it is obvious that $\dot{m}^s_{ji} = \dot{m}^r_{ij}$. $\dot{m}_i$ denotes the fluid flow rate that enters the HES at node i, which is positive for HES in HC modes and negative for HES in HS modes.

Besides, energy conservation at the junctions gives:

HES in HC modes:

$$\sum_{j\to i} \dot{m}^s_{ji}\mathbf{T}_{ji,out} = \mathbf{T}^{s,\mathrm{MIX}}_i \left(\sum_{i\to k} \dot{m}^s_{ik} + \dot{m}_i\right) \tag{23}$$

$$\sum_{k\to i} \dot{m}^r_{ki}\mathbf{T}_{ki,out} + \dot{m}_i\mathbf{T}^{r,\mathrm{PHN}}_i = \mathbf{T}^{r,\mathrm{MIX}}_i \sum_{i\to j} \dot{m}^r_{ij} \tag{24}$$

HES in HS modes:

$$\sum_{j\to i} \dot{m}^s_{ji}\mathbf{T}_{ji,out} - \dot{m}_i\mathbf{T}^{s,\mathrm{PHN}}_i = \mathbf{T}^{s,\mathrm{MIX}}_i \sum_{i\to k} \dot{m}^s_{ik} \tag{25}$$

$$\sum_{k\to i} \dot{m}^r_{ki}\mathbf{T}_{ki,out} = \mathbf{T}^{r,\mathrm{MIX}}_i \left(\sum_{i\to j} \dot{m}^r_{ij} - \dot{m}_i\right) \tag{26}$$

where $\mathbf{T}^{s,\mathrm{MIX}}_i$ and $\mathbf{T}^{r,\mathrm{MIX}}_i$ are temperatures of the mixed flow at the junctions. $\mathbf{T}^{s,\mathrm{PHN}}_i$ and $\mathbf{T}^{r,\mathrm{PHN}}_i$ are the supply and return flow temperature at the primary side of HES at node i. $\mathbf{T}^{s,\mathrm{MIX}}_i = \mathbf{T}^{s,\mathrm{PHN}}_i$ for HC nodes and $\mathbf{T}^{r,\mathrm{MIX}}_i = \mathbf{T}^{r,\mathrm{PHN}}_i$ for HS nodes.

Besides, the safety constraints include:

$$\underline{\dot{m}}_{ij} \le \dot{m}_{ij} \le \overline{\dot{m}}_{ij} \tag{27}$$

$$\underline{\dot{m}}_{i} \le \dot{m}_{i} \le \overline{\dot{m}}_{i} \tag{28}$$

$$\mathbf{T}^{s,\mathrm{PHN}}_i \le \overline{T}_i \tag{29}$$

The pumping cost is considered as:

$$C^{\mathrm{PHN}}_i = \sum_{j\to i} f^{\mathrm{PIPE}}_{ji}(\dot{m}^s_{ij}) + \sum_{k\to i} f^{\mathrm{PIPE}}_{ki}(\dot{m}^r_{ki}) \tag{30}$$

where C^{PHN}_i covers the pumping cost of fluid flow towards node i. $f^{\mathrm{PIPE}}_{ji}(\dot{m}^s_{ij})$ and $f^{\mathrm{PIPE}}_{ki}(\dot{m}^r_{ki})$ are arbitrary convex functions.

The heat exchange between PHN and SHN at the HES is:

$$\mathbf{H}_i = \dot{m}_i c_p \left(\mathbf{T}^{s,\mathrm{PHN}}_i - \mathbf{T}^{r,\mathrm{PHN}}_i\right) \tag{31}$$

Apart from the energy conservation equation above, the heat transfer processes between fluids with different temperatures at the HES and the user-side radiator should be further modelled because they are important to the decisions of flow temperatures and make the optimization problem determinate [28]. The heat transfer constraints will be explained comprehensively in section II-C

C. Modelling of DESs

The DESs are prosumers of power and heat. Considering their relatively small spatial scale, we neglect the power flow constraints and delay and losses of SHN in DESs. Compacting the time-dependent variables into vector forms, the power and heat balance equations are listed as follows:

$$\mathbf{P}_i = \mathbf{P}^l_i + \mathbf{P}^{\mathrm{HP}}_i - \mathbf{P}^{\mathrm{CHP}}_i - \mathbf{P}^{\mathrm{WT}}_i - \mathbf{P}^{\mathrm{PV}}_i \tag{32}$$

$$\mathbf{Q}_i = \mathbf{Q}^l_i - \mathbf{Q}^{\mathrm{CHP}}_i - \mathbf{Q}^{\mathrm{WT}}_i - \mathbf{Q}^{\mathrm{PV}}_i \tag{33}$$

$$w_i\mathbf{H}_i = \mathbf{H}^l_i - \mathbf{H}^{\mathrm{CHP}}_i - \mathbf{H}^{\mathrm{HP}}_i \tag{34}$$

where P, Q and H represent active power, reactive power and heat respectively. The superscript l denotes loads. $\mathbf{P}_i$, $\mathbf{Q}_i$ denote the active and reactive power extracted from the EPN. w_i discriminates between HS and HC nodes by taking -1 or 1. The other terms with superscripts such as CHP represent the generation of corresponding devices. The operational constraints are:

$$\underline{P}^{\mathrm{dev}}_i \le \mathbf{P}^{\mathrm{dev}}_i \le \overline{P}^{\mathrm{dev}}_i, \mathrm{dev} = \mathrm{CHP,\ HP,\ WT\ or\ PV} \tag{35}$$

$$\mathbf{Q}^{\mathrm{dev}}_i = \mathbf{P}^{\mathrm{dev}}_i \tan\varphi^{\mathrm{dev}}_i, \mathrm{dev} = \mathrm{CHP,\ WT\ or\ PV} \tag{36}$$

$$\mathbf{H}^{\mathrm{CHP}}_i = k^{\mathrm{CHP}}_i \mathbf{P}^{\mathrm{CHP}}_i \tag{37}$$

$$\mathbf{H}^{\mathrm{HP}}_i = \mathrm{COP}^{\mathrm{HP}}_i \mathbf{P}^{\mathrm{HP}}_i \tag{38}$$

where φ represent the power angles. k^{CHP}_i is the heat-to-power ratio of CHP i and $\mathrm{COP}^{\mathrm{HP}}_i$ denotes the coefficient of performance of heat pump i. k^{CHP}_i and $\mathrm{COP}^{\mathrm{HP}}_i$ are considered constant.

As for the generation cost, we only consider those of the CHPs and the renewables:

$$\mathbf{C}^{\mathrm{DES}}_i = f^{\mathrm{CHP}}_i\left(\mathbf{P}^{\mathrm{CHP}}_i\right) + \gamma^{\mathrm{WT}}_i\mathbf{P}^{\mathrm{WT}}_i + \gamma^{\mathrm{PV}}_i\mathbf{P}^{\mathrm{PV}}_i \tag{39}$$

where $f^{\mathrm{CHP}}_i(\cdot)$ is a quadratic function. Since $\mathbf{H}^{\mathrm{CHP}}_i$ is coupled with $\mathbf{P}^{\mathrm{CHP}}_i$ through the heat-to-power ratio, $f^{\mathrm{CHP}}_i(\cdot)$ is treated as a univariate function of $\mathbf{P}^{\mathrm{CHP}}_i$. γ is the cost coefficient of the renewable sources and has a small value.

As for the heat transfer process between the PHN and end-users, the nearly proposed heat current method which provides an analogy to linear electrical circuits can be used to characterize them [18]. For completeness, the established model in [28] is reintroduced as follows.

1) Heat current model of HC nodes: Fig. 3(a) presents the heat current model of the SHN in Fig. 1(a) which functions as a PHN heat customer. The heat transfer and temperatures are constrained by:

$$\mathbf{T}^{s,\mathrm{PHN}}_i - \mathbf{T}^{r,\mathrm{SHN}}_i = \mathbf{R}^{\mathrm{HES}}_i \circ \mathbf{H}_i \tag{40}$$

$$\mathbf{T}^{s,\mathrm{SHN}}_i - \mathbf{T}^{\mathrm{room}} \ge \mathbf{R}^{\mathrm{RAD}}_i \circ \mathbf{H}^l_i \tag{41}$$

$$c_p\dot{\mathbf{m}}^{\mathrm{RAD}}_i \circ \left(\boldsymbol{\epsilon}^{\mathrm{HES}}_i + \boldsymbol{\epsilon}^{\mathrm{CHP\text{-}HP}}_i\right) = \mathbf{H}_i + \mathbf{H}^{\mathrm{CHP}}_i + \mathbf{H}^{\mathrm{HP}}_i \tag{42}$$

$$\mathbf{T}^{r,\mathrm{SHN}}_i + \boldsymbol{\epsilon}^{\mathrm{HES}}_i + \boldsymbol{\epsilon}^{\mathrm{CHP\text{-}HP}}_i = \mathbf{T}^{s,\mathrm{SHN}}_i \tag{43}$$

where $\boldsymbol{\epsilon}^{\mathrm{HES}}_i$ and $\boldsymbol{\epsilon}^{\mathrm{CHP\text{-}HP}}_i$ are thermal potentials reflecting temperature increase of fluids in the SHN. $\circ$ represent the element-wise product of vectors. $\mathbf{T}^{s,\mathrm{SHN}}_i$ and $\mathbf{T}^{r,\mathrm{SHN}}_i$ denote

the supply and return temperature of the heat radiator. In (41), we have relaxed the original equality constraint to allow waste of heat.

$\mathbf{R}_i^{\text{HES}}$ and $\mathbf{R}_i^{\text{RAD}}$ are the thermal resistance of the HES and the radiator, and can be represented as a function of the fluid flow rates that enter them, $\dot{\mathbf{m}}_i^{\text{SHN,HES}}$ and $\dot{\mathbf{m}}_i^{\text{RAD}}$:

$$\mathbf{R}_i^{\text{HES}} = R_{\text{HES}}\left(\dot{m}_i, \dot{\mathbf{m}}_i^{\text{SHN,HES}}\right) \tag{44}$$

$$\mathbf{R}_i^{\text{RAD}} = R_{\text{RAD}}\left(\dot{\mathbf{m}}_i^{\text{RAD}}\right) \tag{45}$$

The detailed expressions of nonconvex $R_{\text{HES}}(\cdot)$ and $R_{\text{RAD}}(\cdot)$ can be found in [30] and [18].

2) Heat current model of HS nodes: Fig. 3(b) displays the heat current model of SHN in HS modes. The constraints are:

$$\mathbf{T}_i^{s,\text{SHN}} - \mathbf{T}_i^{r,\text{PHN}} = \mathbf{R}_i^{\text{HES}} \circ \mathbf{H}_i \tag{46}$$

$$\mathbf{T}_i^{s,\text{SHN}} - \mathbf{T}^{\text{room}} \geq \mathbf{R}_i^{\text{RAD}} \circ \mathbf{H}_i^l \tag{47}$$

For simplicity, we assume that the rate of fluid flow that directly enters the end users' heating radiator, i.e., $\dot{\mathbf{m}}_i^{\text{RAD}}$, cannot be freely adjusted, while the flow rate that enters the HES at the SHN side, i.e., $\dot{\mathbf{m}}_i^{\text{SHN,HES}}$, can be regulated within a given range $\left[\underline{\dot{m}_i^{\text{SHN,HES}}}, \overline{\dot{m}_i^{\text{SHN,HES}}}\right]$. Therefore, (40) and (46) can be equivalently rewritten for HC and HS nodes respectively as follows:

$$\underline{R_i^{\text{HES}}}(\dot{m}_i)\mathbf{H}_i \leq \mathbf{T}_i^{s,\text{PHN}} - \mathbf{T}_i^{r,\text{SHN}} \leq \overline{R_i^{\text{HES}}}(\dot{m}_i)\mathbf{H}_i \tag{48}$$

$$\underline{R_i^{\text{HES}}}(\dot{m}_i)\mathbf{H}_i \leq \mathbf{T}_i^{s,\text{SHN}} - \mathbf{T}_i^{r,\text{PHN}} \leq \overline{R_i^{\text{HES}}}(\dot{m}_i)\mathbf{H}_i \tag{49}$$

where $\underline{R_i^{\text{HES}}}(\dot{m}_i)$ and $\overline{R_i^{\text{HES}}}(\dot{m}_i)$ are calculated by substituting $\overline{\dot{m}_i^{\text{SHN,HES}}}$ and $\underline{\dot{m}_i^{\text{SHN,HES}}}$ into (44) respectively.

D. Modelling of Electric Power System

The power grid that connects the DESs is assumed to be a radial distribution network. According to the second-order-cone relaxed distflow model [31], [32], the constraints are:

$$\sum_{j:j\to i} \mathbf{P}_{ji} = \sum_{i:i\to k} (\mathbf{P}_{ik} + \mathbf{l}_{ik} R_{ik}) + \mathbf{P}_i \tag{50}$$

$$\sum_{j:j\to i} \mathbf{Q}_{ji} = \sum_{i:i\to k} (\mathbf{Q}_{ik} + \mathbf{l}_{ik} X_{ik}) + \mathbf{Q}_i \tag{51}$$

$$\mathbf{v}_i = \mathbf{v}_j - 2\left(R_{ji}\mathbf{P}_{ji} + X_{ji}\mathbf{Q}_{ji}\right) + \left(R_{ji}^2 + X_{ji}^2\right)\mathbf{l}_{ji} \tag{52}$$

$$\mathbf{l}_{ji} \circ \mathbf{v}_i \geqslant \mathbf{P}_{ji}^2 + \mathbf{Q}_{ji}^2 \tag{53}$$

The direction $j \to i$ indicates that node j is the parent of i in the tree-like grid. $\mathbf{P}_{ji}$ and $\mathbf{Q}_{ji}$ denote power flow, while $\mathbf{P}_i$ and $\mathbf{Q}_i$ represent the net active and reactive power loads of node i. $\mathbf{v}$ and $\mathbf{l}$ are the squared magnitudes of nodal voltage and transmission line current. The safety constraints are:

$$\underline{v_i} \leq \mathbf{v}_i \leq \overline{v_i} \tag{54}$$

$$\mathbf{l}_{ij} \leq \overline{l_{ij}} \tag{55}$$

To sum up, the dispatch problem for the DESs minimizes the following objective:

$$\min \sum_i C_i = \sum_i \left(\mathbf{1}^{\text{T}}\mathbf{C}_i^{\text{DES}} + C_i^{\text{PHN}}\right) \tag{56}$$

The constraints include: 1) PHN constraints: (18), (20)-(29); 2) DES and SHN constraints: (32)-(34), (41)-(44), (47)-(49); 3) EPN constraints: (50)-(55).

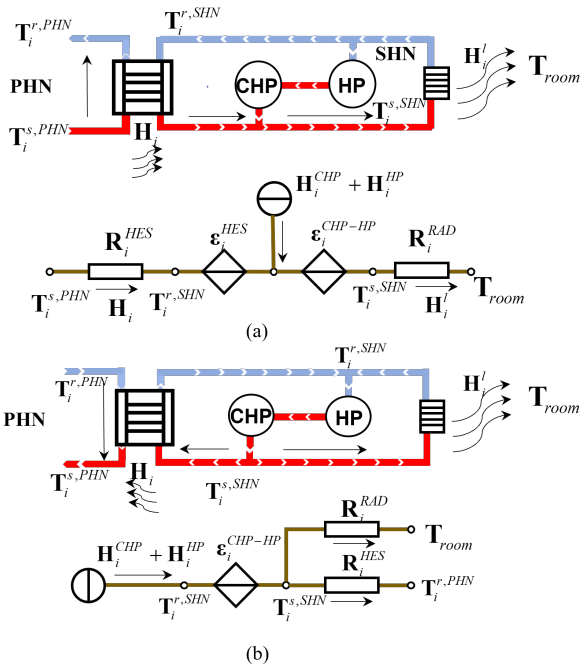

Fig. 3. Heat current model of the secondary heating network: (a) SHN in HC modes. PHN and local devices provide heat to the users. (b) SHN in HS modes. Local devices provide heat to the PHN and users. The temperatures nodes are labelled in the SHN to illustrate its relationship with the heat current diagram.

III. Fully Decentralized Solution Method

A. Description of the algorithm

Considering the multi-agent structure of networked DESs, decentralized optimization methods are considered. Typical decentralized algorithms include dual decomposition method [33], ADMM [34], and optimality condition decomposition methods [35], which split the optimization problem into several subproblems and solve them iteratively. Generally, the methods are designed for convex problems. However, the model introduced in section II reveals strong nonlinear properties. Specifically, (18), (31), (48) and (49) are complicated nonconvex constraints. Therefore, a direct application of popular decentralized methods may face great difficulties.

Despite the obstacles, it can be observed that all the constraints are convex when the fluid flow rates are fixed. Besides, the constraints related only to fluid flow rates, i.e., (21), (22), (27) and (28), are very simple. These properties inspire a primal-decomposition-based optimization method. In primal decomposition, the complicated decision variables are fixed so that we can easily solve the rest problem and provide guidance for the update of complicated variables. In this work, we denote the complicated decisions of PHN fluid flow rates as $\mathbf{Y}$ and the rest decision variables as $\mathbf{X}$. For easy reference, the optimization model is compacted to the following form:

$$\min \sum_{i=1}^{N} C_i\left(\mathbf{X}_i, \mathbf{Y}_i\right) \tag{57a}$$

$$\text{s.t. } \mathbf{X}_i \in \mathcal{G}_{\mathbf{Y}_i, i} \tag{57b}$$

$$\mathbf{Y} \in \mathcal{H} \tag{57c}$$

$$\mathbf{C}_{ij}\mathbf{X}_i+\mathbf{C}_{ji}\mathbf{Z}_j = \mathbf{0} \tag{57d}$$

$$\mathcal{G}_{\mathbf{Y}_i,i} = \{\mathbf{X}_i|\mathbf{G}_i^1(\mathbf{X}_i,\mathbf{Y}_i)=0,\ \mathbf{G}_i^2(\mathbf{X}_i,\mathbf{Y}_i)\le 0\} \tag{57e}$$

$$\mathcal{H} = \{\mathbf{Y}|\mathbf{H}^1\mathbf{Y}=0,\mathbf{H}^2\mathbf{Y}\le 0\} \tag{57f}$$

$$(i,j)\in\mathcal{E}\ ,\ i=0,1,...,N-1$$

where $\mathbf{X}_i$ and $\mathbf{Y}_i$ collects specific decision variables concerning DES node i. The variables with subscript ij in the model are involved in both $\mathbf{X}_i(\mathbf{Y}_i)$ and $\mathbf{X}_j(\mathbf{Y}_j)$. Besides, we introduce $\mathbf{Z}_i$ as a duplication of $\mathbf{X}_i$. The constraint (57d) ensures both consistency between $\mathbf{X}_i$ and $\mathbf{Z}_i$, as well as between $\mathbf{X}_i$ and $\mathbf{X}_j$. $\mathbf{C}_{ij}$ is the coupling matrix whose elements can only be 0, 1 or -1. Different rows of (57d) may indicate consistency of transmission line power, nodal voltages or temperatures respectively. $(i,j)\in\mathcal{E}$ indicates that DES i and j are connected with a transmission line or PHN pipelines. Besides, (57c) indicates both the consistency constraints and safety and conservation constraints of fluid flow rates, where $\mathcal{H}$ is a convex set. $\mathcal{G}_{\mathbf{Y}_i,i}$ imposes DES local constraints on $\mathbf{X}_i$ and is convex for arbitrary fixed $\mathbf{Y}_i$.

Relaxing coupling constraints (57d) and fixing $\mathbf{Y}$, the partial augmented lagrangian is given as:

$$L(\mathbf{X},\mathbf{Y},\mathbf{Z},\boldsymbol{\lambda}) = \sum_{i=1}^{N} C_i(\mathbf{X}_i,\mathbf{Y}_i) + \sum_{\substack{\forall i,\forall j\\(i,j)\in\mathcal{E}}}\left[\boldsymbol{\lambda}_{ij}^T(\mathbf{C}_{ij}\mathbf{X}_i+\mathbf{C}_{ji}\mathbf{Z}_j)+\frac{1}{2}\|\mathbf{C}_{ij}\mathbf{X}_i+\mathbf{C}_{ji}\mathbf{Z}_j\|_\Theta^2\right] \tag{58}$$

where Θ is a diagonal matrix with positive elements and its dimension equals to that of $\mathbf{C}_{ij}\mathbf{X}_i+\mathbf{C}_{ji}\mathbf{Z}_j$. $\|\cdot\|_\Theta^2$ is the quadratic form determined by Θ, i.e., $\|a\|_\Theta^2 \triangleq a^T\Theta a$.

By minimizing over $\mathbf{X}$ and $\mathbf{Z}$ and maximizing over $\boldsymbol{\lambda}$, the optimal dual objective is:

$$\xi(\mathbf{Y}) = \max_{\boldsymbol{\lambda}}\psi(\mathbf{Y},\boldsymbol{\lambda}) = \max_{\boldsymbol{\lambda}}\min_{\mathbf{Z}_i,\mathbf{X}_i\in\mathcal{G}_{\mathbf{Y}_i,i}} L(\mathbf{X},\mathbf{Y},\mathbf{Z},\boldsymbol{\lambda}) \tag{59}$$

which is also the optimal value of problem (57) for a given $\mathbf{Y}$. Herein, the basic idea is to employ ADMM to obtain an approximate value of $\xi(\mathbf{Y})$ and then apply decentralized gradient descent to update $\mathbf{Y}$. In ADMM, the objective function for each DES agent i is given by decomposing the partial augmented lagrangian (58):

$$L_i(\mathbf{X}_i,\mathbf{Y}_i,\mathbf{Z}_i,\boldsymbol{\lambda}_i) = C_i(\mathbf{X}_i,\mathbf{Y}_i) + \sum_{\substack{\forall j\\(i,j)\in\mathcal{E}}}\left[\boldsymbol{\lambda}_{ij}^T(\mathbf{C}_{ij}\mathbf{X}_i+\mathbf{C}_{ji}\mathbf{Z}_j)+\frac{1}{2}\|\mathbf{C}_{ij}\mathbf{X}_i+\mathbf{C}_{ji}\mathbf{Z}_j\|_\Theta^2\right] \tag{60}$$

where $\boldsymbol{\lambda}_i$ collects the multipliers $\boldsymbol{\lambda}_{ij}$ for $(i,j)\in\mathcal{E}$.

The decentralized optimization framework is given in **Algorithm 1**. In *x-update*, each DES agent minimizes (60) to obtain $\mathbf{X}_i^{(k)}$ with given $\mathbf{Z}_i^{(k-1)}$ and $\mathbf{Z}_j^{(k-1)}$ collected from neighbours. In *z-update*, $\mathbf{Z}_i^{(k)}$ is calculated by minimizing (60) given $\mathbf{X}_i^{(k)}$ and $\mathbf{X}_j^{(k)}$ from neighbours. After optimizing the primal variables $\mathbf{X}_i$ and $\mathbf{Z}_i$ alternately, the multipliers are then updated through dual ascent. It should be noted that the fluid flow rates $\mathbf{Y}_i$ are not updated directly in **Algorithm 1**. Instead, a relatively loose threshold ϵ_1^{tol} is used to estimate the calculation accuracy of $\xi(\mathbf{Y})$ and **Algorithm 2** is employed to update $\mathbf{Y}_i$ for PHN nodes.

Algorithm 1 Decentralized Optimization Framework

1: **Initialize**
   Set $k:=0$, residual tolerances $\epsilon_1^{\text{tol}} > \epsilon_2^{\text{tol}}$
   Each agent i sets arbitrary initial $\mathbf{Z}_i^{(0)}$ and multipliers $\lambda_{ij}^{(0)}$ for $\forall j\in\mathcal{N}_i$ and a feasible initial $\mathbf{Y}_i^{(0)}$
2: **repeat**
3: **for** agent i=0,1,...,$N-1$ parallelly **do**
4: (*x-update*)
5: Collect $\mathbf{Z}_j^{(k)}$ and $\boldsymbol{\lambda}_{ij}^{(k)}$ from each node $j\in\mathcal{N}_i$
6: Minimize $L_i\left(\mathbf{X}_i,\mathbf{Y}_i^{(k)},\mathbf{Z}_i^{(k)},\boldsymbol{\lambda}_i^{(k)}\right)$ to obtain the minimizer $\mathbf{X}_i{}^{(k+1)}\in\mathcal{G}_{\mathbf{Y}_i^{(k)},i}$
7: (*z-update*)
8: Collect $\mathbf{X}_j^{(k+1)}$ from each node $j\in\mathcal{N}_i$
9: Minimize $L_i\left(\mathbf{X}_i{}^{(k+1)},\mathbf{Y}_i^{(k)},\mathbf{Z}_i,\boldsymbol{\lambda}_i^{(k)}\right)$ to obtain the minimizer $\mathbf{Z}_i{}^{(k+1)}$.
10: (*Dual ascent of the multipliers*)
11: $\boldsymbol{\lambda}_{ij}^{(k+1)} := \boldsymbol{\lambda}_{ij}^{(k)} + \Theta\left(\mathbf{C}_{ij}\mathbf{X}_i^{(k+1)}+\mathbf{C}_{ji}\mathbf{Z}_j^{(k+1)}\right)$ for $\forall j\in\mathcal{N}_i$
12: Calculate the primal and dual residuals of $\mathbf{X}_i$:
$R_{p,i}^{(k+1)} := \|\mathbf{C}_{ij}\mathbf{X}_i^{(k+1)}+\mathbf{C}_{ji}\mathbf{Z}_j^{(k+1)}\|_\infty$
$R_{d,i}^{(k+1)} := \|\mathbf{X}_i^{(k+1)}-\mathbf{X}_i^{(k)}\|_\infty$
13: **if** not converge with the looser tolerance ϵ_1^{tol} **then**
14: Broadcast partial update signals in the system.
15: **else**
16: Broadcast full update signals in the system.
17: **end if**
18: **if** partial update signals received **then**
19: $\mathbf{Y}_i^{(k+1)} := \mathbf{Y}_i^{(k)}$
20: **else**
21: Execute **Algorithm 2** for PHN nodes to obtain $\mathbf{Y}_i^{(k+1)}$ and the residual $R_{\mathbf{Y}_i}^{(k+1)}$ of $\mathbf{Y}_i$.
22: **end if**
23: **if** $\mathbf{X}_i$ and $\mathbf{Y}_i$ not converge with threshold ϵ_2^{tol} **then**
24: Broadcast signals of continuous iteration.
25: **end if**
26: **end for**
27: **until** No iteration signals are broadcast and received

Algorithm 2 can be divided into three parts: the decentralized gradient calculation from step 4 to 13, the decentralized step size calculation from step 14 to 25, and the gradient descent part from step 26 to 29.

In the gradient calculation part, since the residuals of $\mathbf{X}$ and $\boldsymbol{\lambda}$ have been small enough, we can safely estimate that:

$$\begin{aligned}\xi^{(k)} &\triangleq \xi\left(\mathbf{Y}^{(k)}\right) \approx L\left(\mathbf{X}^{(k+1)},\mathbf{Y}^{(k)},\mathbf{Z}^{(k+1)},\boldsymbol{\lambda}^{(k+1)}\right)\\ &= \sum_{i=1}^{N} L_i^{(k)} = \sum_{i=1}^{N} L_i\left(\mathbf{X}_i^{(k+1)},\mathbf{Y}_i^{(k)},\mathbf{Z}^{(k+1)},\boldsymbol{\lambda}_i^{(k+1)}\right)\end{aligned} \tag{61}$$

It should be noted that $\mathbf{Y}\in\mathcal{H}$ indicates that the terms in $\mathbf{Y}$ are not independent. Therefore, we select $\dot{m}_i, i\neq l_0$ as

Algorithm 2 Decentralized Gradient Descent of $\mathbf{Y}$

1: **Assumptions**
The PHN is a radial connected network. One arbitrary PHN node is taken as a slack node(l_0).
2: **Initialize**
Let $b_{ij}=1$ if water flows from node i to j in the supply PHN and $b_{ij}=-1$ for the opposite case. Let $t_i=1$ if DES node i is a HS node and $t_i=-1$ if i is a HC node.
Set auxiliary $a_i=a_{ij}=0$. Set gradients $c_i=0$.
Set auxiliary $s_i^{\max}=s_{ij}^{\max}=d_{ij}=0$.
Set the reference step size s^{ref}, $\gamma\in(0,1)$, and actual step size of gradient descent $s=0$
3: **for** each PHN agent i=l_0, l_1, ..., l_{N_h-1} parallelly **do**
4: (*Decentralized calculation of gradients*)
5: Calculate $\frac{\partial\xi_i^{(k)}}{\partial\mathbf{Y}_i^{(k)}}$, i.e., calculate $\frac{\partial\xi_i^{(k)}}{\partial\dot{m}_i^{(k)}}$ and $\frac{\partial\xi_i^{(k)}}{\partial\dot{m}_{ij}^{(k)}}$.
6: **if** i is the slack node l_0 **then**
7: $a_i:=t_i\frac{\partial\xi_i^{(k)}}{\partial\dot{m}_i^{(k)}}$,
8: **else**
9: Wait for a_{u_ii} from some neighbour node u_i.
10: $a_i:=a_{u_ii}+b_{u_ii}\frac{\partial\xi_i^{(k)}}{\partial\dot{m}_{u_ii}^{(k)}}$, $c_i:=-t_ia_i+\frac{\partial\xi_i^{(k)}}{\partial\dot{m}_i^{(k)}}$.
11: **end if**
12: $a_{ij}:=a_i+b_{ij}\frac{\partial\xi_i^{(k)}}{\partial\dot{m}_{ij}^{(k)}}$.
13: Send a_{ij} to each PHN neighbour $j\in\mathcal{N}_i^h$.
14: (*Decentralized calculation of the step size*)
15: Wait for d_{ij} and $s_{ij}^{\max}$ from each $j\in\mathcal{N}_i^h$ except u_i.
16: $s_i'^{\max}:=\max\{s|\underline{\dot{m}}_i\le\dot{m}_i^{(k)}-sc_i\le\overline{\dot{m}}_i\}$
17: $s_i^{\max}:=\min\{s_i'^{\max},s_{ij}^{\max}\}$ for all $j\in\mathcal{N}_i^h$
18: **if** i is NOT the slack node l_0 **then**
19: $d_{u_ii}:=b_{u_ii}(t_ic_i+\sum_{j\in\mathcal{N}_i^h,j\neq u_i}b_{ij}d_{ij})$
20: $s_{u_ii}'^{\max}:=\max\{s|\underline{\dot{m}}_{u_ii}\le\dot{m}_{u_ii}^{(k)}+sd_{u_ii}\le\overline{\dot{m}}_{u_ii}\}$.
21: $s_{u_ii}^{\max}:=\min\{s_{u_ii}'^{\max},s_i^{\max}\}$.
22: Send d_{u_ii} and $s_{u_ii}^{\max}$ to node u_i
23: **else**
24: $s:=\min\{s_i'^{\max},s^{\text{ref}}/(1+\gamma*k)\}$, broadcast s.
25: **end if**
26: (*Residuals*): $R_{\mathbf{Y}_i}^{(k+1)}:=|sc_i|$
27: (*Gradient descent*) $\dot{m}_i^{(k+1)}:=\dot{m}_i^{(k)}-sc_i$
28: (*Update* $\mathbf{Y}^{(k+1)}$) Wait for $\dot{m}_j^{(k+1)}$ from $j\in\mathcal{N}_i^h$ except u_i, update $\dot{m}_{ij}^{(k+1)}$ according to mass conservation, and send $\dot{m}_i^{(k+1)}$ to u_i
29: **end for**

independent decision variables and estimates their impacts on $\xi^{(k)}$ by calculating the gradients c_i through the chain rule,

$$\begin{aligned}c_i&\triangleq\frac{\partial\xi^{(k)}}{\partial\dot{m}_i^{(k)}}\\&=\sum_{j=l_0}^{l_{N_h-1}}\left(\frac{\partial L_j^{(k)}}{\partial\mathbf{Y}_j^{(k)}}+\boldsymbol{\mu}_{\mathbf{A}_j}^{(k)T}\frac{\partial\mathbf{A}_j^{(k)}}{\partial\mathbf{Y}_j^{(k)}}\right)^T\frac{\partial\mathbf{Y}_j^{(k)}}{\partial\dot{m}_i^{(k)}}\end{aligned}\tag{62}$$

where $\mathbf{A}_j^{(k)}$ collects all active constraints in $\mathcal{G}_{\mathbf{Y}_j,j}$ and $\boldsymbol{\mu}_{\mathbf{A}_j}^{(k)}$ denotes the corresponding multipliers. l_0, ..., l_{N_h-1} are indices of DESs connected to the PHN. For brevity, we define the terms in the brackets as $\frac{\partial\xi_j^{(k)}}{\partial\mathbf{Y}_j^{(k)}}$. In **Algorithm 2**, they are first locally calculated at step 5. Then auxiliary variables a_i, a_{ij}, t_i and b_{ij} are introduced to calculate c_i in a fully decentralized manner.

In the step size calculation part, each agent i estimates the maximum step size from step 14 to 21 and sends it to u_i. To ensure the primal feasibility of $\mathbf{Y}_i$, the minimum of candidate step sizes is calculated at the slack node as s and broadcast to the entire system in step 24. Note that we use a parameter γ to give decreasing step sizes.

In step 26-29, every DES node performs the gradient descent for $\dot{m}_i$ and update $\dot{m}_{ij}$ according to the constraints.

A detailed illustration of how these calculation processes are designed is presented in [30]. It should be noted that, in **Algorithm 2**, some calculations, e.g., step 10 and 16, must be performed after a certain message is received. These communications and calculations are asynchronized and not completely parallelable. However, they only involve waiting for several real numbers and simple addition/subtraction/comparison operations. Therefore, the asynchronization would not lead to expensive communication cost under the decentralized framework.

B. Convergence Analysis

The proposed method can actually be seen as doing inexact gradient descent on $\xi(\mathbf{Y})$. Indeed, we have,

$$\nabla\xi(\mathbf{Y})=\frac{L(\mathbf{X}^*,\mathbf{Y},\mathbf{Z}^*,\boldsymbol{\lambda}^*)}{\partial\mathbf{Y}}\tag{63}$$

where superscript $*$ denotes the optimizer for given $\mathbf{Y}$. We estimate $\nabla\xi(\mathbf{Y})$ by:

$$\nabla\xi(\mathbf{Y})_{est}^{(k)}=\frac{L\left(\mathbf{X}^{(k)},\mathbf{Y},\mathbf{Z}^{(k)},\boldsymbol{\lambda}^{(k)}\right)}{\partial\mathbf{Y}}\tag{64}$$

It is obvious that,

$$\begin{aligned}\nabla\xi(\mathbf{Y})-\nabla\xi(\mathbf{Y})_{est}^{(k)}=&\sum_{i=0}^{N-1}\left(\frac{\partial C_i(\mathbf{X}^*,\mathbf{Y})}{\partial\mathbf{Y}}-\frac{\partial C_i\left(\mathbf{X}^{(k)},\mathbf{Y}\right)}{\partial\mathbf{Y}}\right)\\&+\sum_{j=l_0}^{l_{N_h-1}}\left(\boldsymbol{\mu}_{\mathbf{G}_j^1}^*\frac{\partial\mathbf{G}_j^1\left(\mathbf{X}_j^*,\mathbf{Y}_j\right)}{\partial\mathbf{Y}}-\boldsymbol{\mu}_{\mathbf{G}_j^1}^{(k)}\frac{\partial\mathbf{G}_j^1\left(\mathbf{X}_j^{(k)},\mathbf{Y}_j\right)}{\partial\mathbf{Y}}\right)\\&+\sum_{j=l_0}^{l_{N_h-1}}\left(\boldsymbol{\mu}_{\mathbf{G}_j^2}^*\frac{\partial\mathbf{G}_j^2\left(\mathbf{X}_j^*,\mathbf{Y}_j\right)}{\partial\mathbf{Y}}-\boldsymbol{\mu}_{\mathbf{G}_j^2}^{(k)}\frac{\partial\mathbf{G}_j^2\left(\mathbf{X}_j^{(k)},\mathbf{Y}_j\right)}{\partial\mathbf{Y}}\right)\end{aligned}\tag{65}$$

where $\boldsymbol{\mu}_{\mathbf{G}_j^1}$ and $\boldsymbol{\mu}_{\mathbf{G}_j^2}$ are multipliers of local constraints $\mathbf{G}_i^1(\mathbf{X}_i,\mathbf{Y}_i)=0$ and $\mathbf{G}_i^2(\mathbf{X}_i,\mathbf{Y}_i)\le0$ in (57b).

Recall that the cost function $C_i(\cdot)$ is a quadratic one but does not involve cross terms of $\mathbf{X}$ and $\mathbf{Y}$. Therefore, the first terms of (65) can be cancelled. Besides, $\mathbf{X}$ and $\mathbf{Y}$ in the nonconvex local constraints $\mathbf{G}_i^1(\mathbf{X}_i,\mathbf{Y}_i)=0$ and $\mathbf{G}_i^2(\mathbf{X}_i,\mathbf{Y}_i)\le0$ are separable according to the modelling. Then we have,

$$\mathbf{G}_j^1(\mathbf{X}_j,\mathbf{Y}_j)=\mathbf{G}_j^{1-1}(\mathbf{Y}_j)\mathbf{X}+\mathbf{G}_j^{1-2}(\mathbf{Y}_j)\tag{66}$$

$$\mathbf{G}_j^2(\mathbf{X}_j,\mathbf{Y}_j)=\mathbf{G}_j^{2-1}(\mathbf{Y}_j)\mathbf{X}+\mathbf{G}_j^{2-2}(\mathbf{Y}_j)\tag{67}$$

Substituting (66) and (67) into (65), we then obtain that,

$$\begin{aligned}
&\left\|\nabla\xi\left(\mathbf{Y}\right)-\nabla\xi\left(\mathbf{Y}\right)_{est}^{(k)}\right\| \\
\leq&\sum_{j=l_0}^{l_{N_h}-1}\left\|\left(\boldsymbol{\mu}_{\mathbf{G}_j^1}^{*}-\boldsymbol{\mu}_{\mathbf{G}_j^1}^{(k)}\right)^T\left(\frac{\partial\mathbf{G}_j^{1-1}(\mathbf{Y}_j)}{\partial\mathbf{Y}}\mathbf{X}^*+\frac{\partial\mathbf{G}_j^{1-2}(\mathbf{Y}_j)}{\partial\mathbf{Y}}\right)\right\| \\
+&\sum_{j=l_0}^{l_{N_h}-1}\left\|\boldsymbol{\mu}_{G_j^1}^{(k)T}\frac{\partial\mathbf{G}_j^{1-1}(\mathbf{Y}_j)}{\partial\mathbf{Y}}\left(\mathbf{X}^*-\mathbf{X}_j^{(k)}\right)\right\| \\
+&\sum_{j=l_0}^{l_{N_h}-1}\left\|\left(\boldsymbol{\mu}_{\mathbf{G}_j^2}^{*}-\boldsymbol{\mu}_{\mathbf{G}_j^2}^{(k)}\right)^T\left(\frac{\partial\mathbf{G}_j^{2-1}(\mathbf{Y}_j)}{\partial\mathbf{Y}}\mathbf{X}^*+\frac{\partial\mathbf{G}_j^{2-2}(\mathbf{Y}_j)}{\partial\mathbf{Y}}\right)\right\| \\
+&\sum_{j=l_0}^{l_{N_h}-1}\left\|\boldsymbol{\mu}_{G_j^1}^{(k)T}\frac{\partial\mathbf{G}_j^{2-1}(\mathbf{Y}_j)}{\partial\mathbf{Y}}\left(\mathbf{X}^*-\mathbf{X}_j^{(k)}\right)\right\| \\
\leq& O\left(\left\|\boldsymbol{\mu}_{\mathbf{G}_j^1}^{*}-\boldsymbol{\mu}_{\mathbf{G}_j^1}^{(k)}\right\|+\left\|\boldsymbol{\mu}_{\mathbf{G}_j^2}^{*}-\boldsymbol{\mu}_{\mathbf{G}_j^2}^{(k)}\right\|+\left\|\mathbf{X}^*-\mathbf{X}_j^{(k)}\right\|\right)
\end{aligned} \tag{68}$$

where the last inequality is based on the fact that the partial derivatives in terms of $\mathbf{Y}$ all have analytical expressions and $\mathbf{Y}$ is bounded during the optimization.

Suppose that we are doing gradient descent for $\mathbf{Y}$ in a neighbourhood of $\mathbf{Y}^*$, which is a local optimizer of $\xi(\mathbf{Y})$, and that $\xi(\mathbf{Y})$ is $m-$*strongly convex* with $M-$*Lipschitz continuous* gradients [36] in this neighbourhood of $\mathbf{Y}^*$, and then we obtain $\|\nabla\xi(\mathbf{Y})\| \geq m\|\mathbf{Y}-\mathbf{Y}^*\|$. According to (68), for $\forall\|\mathbf{Y}-\mathbf{Y}^*\| \geq \epsilon$ and some $\delta\in(0,1)$ there exists a small threshold ϵ_1^{tol} to control the convergence of ADMM and ensure that $\left\|\nabla\xi\left(\mathbf{Y}\right)-\nabla\xi\left(\mathbf{Y}\right)_{est}^{(k)}\right\| \leq \delta m\epsilon \leq \delta m\|\mathbf{Y}-\mathbf{Y}^*\| \leq \delta\|\nabla\xi(\mathbf{Y})\|$ for some k. Then from proposition 1.4 of [36] we know that a proper descent step size also exists which ensures the convergence of the proposed inexact gradient descent to the ϵ-*neighbourhood* of $\mathbf{Y}^*$. A smaller ϵ_1^{tol} would bring about a more accurate calculation of $\mathbf{Y}^*$.

Actually, the analysis above is more conservative as [36] considers gradient calculation with possibly adversarially chosen errors. In the proposed method, the gradients calculations are inexact with respect to $\xi\left(\mathbf{Y}\right)$ but still give the exact descent direction of the lagrangian function $L\left(\mathbf{X}^{(k)},\mathbf{Y},\mathbf{Z}^{(k)},\boldsymbol{\lambda}^{(k)}\right)$. Therefore, the actual convergence may be better than the analysis.

However, the actual property of $\xi(\mathbf{Y})$ is hard to analyze in real energy systems, and to ensure the ultimate convergence of $\mathbf{Y}^{(k)}$ we use a decreasing step size through the parameter γ. In the case study, we use two test systems to show the effectiveness of the proposed method with some simple choice of the parameters.

IV. Case Study

A. Comparisons of the proposed model and the node method

We first compare the proposed model and the node method with the numerical solution of partial differential equations for a 9.1 km pipeline. Fig. 4 presents the result. The PHN fluid flow rates and the inlet temperatures are manually given. It can be observed that the results of the two methods are both quite close to the numerical solutions. When the pipeline delay time is an integer multiple of the dispatch time step, e.g., when t<0 or t=10-23 in Fig. 4(a), the outlet flow temperatures given by different methods are identical. When the delay time is not an integer multiple of Δt, or when the fluid flow rates encounter a sudden change, the decision of flow temperatures may have a max difference of 2-3K. Nevertheless, the trends of the calculation results are highly consistent.

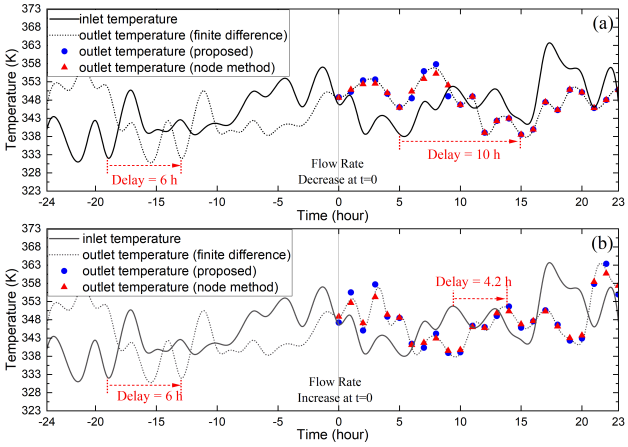

Fig. 4. Comparisons of the proposed model and the node method with the numerical solution of pipeline flow through finite difference method. The fluid flow rates and the inlet temperatures are manually given. Two cases are considered: (a) fluid flow rates decrease at t=0. (b) fluid flow rates increase at t=0. Note that we are only concerned about $t \geq 0$

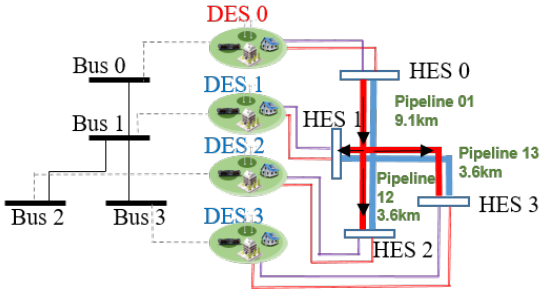

Fig. 5. The sketch of 4-DES system.

B. 4-node Test System

Fig. 5 shows the sketch of a test system composed of 4 DESs, each possibly equipped with a micro gas-fired CHP, a HP or renewable sources. The SHNs are the same as those in Fig. 3 and are omitted here. The EPN and PHN are strongly coupled by the DESs, which are coordinated in a decentralized manner. DES 0 is a HS node and provides heat to the other 3 DESs through the PHN. The other DESs serving as heat customers can also flexibly adjust their heat extraction from the PHN by running local CHPs and HPs as a supplementary. The time step of day-ahead dispatch is 1 hour.

Table I lists the system parameters, including generation limits of CHPs and HPs, the heat-to-power ratios and COPs, historical fluid flow rates along with their adjustment ranges, and some parameters used in the decentralized numerical calculation. In ADMM, the transmission line power is initialized to 0, and the squared magnitude of voltages are initialized to 1. The temperatures are initialized to their historical values and all of the multipliers are initialized to 0. Besides, recall that the elements of Θ in (60) defines different quadratic penalty terms for different constraints. In this paper, the diagonal element

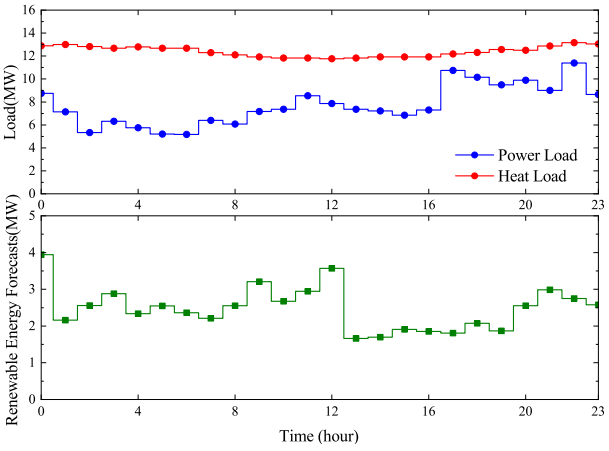

Fig. 6. Power and heat loads and renewable energy forecasts.

TABLE I
PARAMETERS USED IN THE CALCULATION

Item	Value	Item	Value
$[\underline{P_0^{\text{CHP}}}, \overline{P_0^{\text{CHP}}}]$	$[2, 8]$MW	k_0^{CHP}	2
$[\underline{P_1^{\text{CHP}}}, \overline{P_1^{\text{CHP}}}]$	$[0.4, 1.6]$MW	k_1^{CHP}	1
$[\underline{P_2^{\text{CHP}}}, \overline{P_2^{\text{CHP}}}]$	$[0.8, 3.2]$MW	k_2^{CHP}	1
$[\underline{P_3^{\text{CHP}}}, \overline{P_3^{\text{CHP}}}]$	$[0.4, 1.6]$MW	k_3^{CHP}	1
$[\underline{P_1^{\text{HP}}}, \overline{P_1^{\text{HP}}}]$	$[0, 0.43]$MW	COP_1^{HP}	1.4
$[\underline{P_2^{\text{HP}}}, \overline{P_2^{\text{HP}}}]$	$[0, 0.43]$MW	COP_2^{HP}	1.4
$[\underline{P_3^{\text{HP}}}, \overline{P_3^{\text{HP}}}]$	$[0, 0.43]$MW	COP_3^{HP}	1.4
$f_0^{\text{CHP}}(\cdot)$	$2x^2 + 440x$	$f_1^{\text{CHP}}(\cdot)$	$25x^2 + 370x$
$f_2^{\text{CHP}}(\cdot)$	$25x^2 + 370x$	$f_3^{\text{CHP}}(\cdot)$	$25x^2 + 370x$
$\dot{m}_1^{\text{his}}$	50.89kg/s	$[\underline{\dot{m}_1}, \overline{\dot{m}_1}]$	$[25.45, 76.33]$kg/s
$\dot{m}_2^{\text{his}}$	50.89kg/s	$[\underline{\dot{m}_2}, \overline{\dot{m}_2}]$	$[25.45, 76.33]$kg/s
$\dot{m}_3^{\text{his}}$	50.89kg/s	$[\underline{\dot{m}_3}, \overline{\dot{m}_3}]$	$[25.45, 76.33]$kg/s
$[\underline{\dot{m}_{01}}, \overline{\dot{m}_{01}}]$	$[76.34, 229.02]$kg/s	γ	0.001
$[\underline{\dot{m}_{12}}, \overline{\dot{m}_{12}}]$	$[25.45, 76.34]$kg/s	ϵ_1^{tol}	0.2MW/0.2K
$[\underline{\dot{m}_{13}}, \overline{\dot{m}_{13}}]$	$[25.45, 76.34]$kg/s	ϵ_2^{tol}	0.005MW/0.01K
s^{ref}	0.01	$\overline{T}_i$	363K(90°C)

takes 50 if it relates to a consistency constraint of power flow and takes 10 if relates to that of flow temperatures or nodal voltages. These values can be updated through an adaptive [37] method but we do not include it in our work. More detailed data is provided in [30]. Profiles of total power and heat loads and renewable energy forecasts are shown in Fig. 6. The subproblem of each DES is solved with ECOS [38] on a 3.4GHz PC with 8GB of memory.

C. Performance of the Decentralized Optimization Method

Fig. 7 displays the convergence trajectories when the proposed decentralized dispatch method is employed. According to Fig. 7(a), the objective cost function and lagrangian function converges in 1500 iterations. The residuals also drop to the thresholds in about 1200 iterations as illustrated by Fig. 7(c) and (d). The decisions of fluid flow rates are shown in Fig. 7(b). In the first 400 iterations, the fluid flow rates present a stairlike variation because the high residuals prevent frequent executions of algorithm 2. As the iteration continues, the residuals reach a low level and the complicated decision variables are then updated in company with the multipliers and simple decision variables in each iteration.

Another two direct applications of ADMM(ADMM-1, ADMM-2) to solve the dispatch problem is also realized and compared with the proposed method. In ADMM-1, the fluid flow rates are not updated, i.e., algorithm 2 is not executed. In ADMM-2, the fluid flow rates are also included in the augmented lagrangian formulation in (60) and fluid flow rates are directly updated in each subproblem instead of using the proposed method. Noting that the subproblem is highly nonconvex and most open-source of commercial solvers may fail, we solve the subproblem using Generalized Benders Decomposition(GBD) [39] with a duality gap of 0.1. The simple variables rather than the complicated flow rates are optimized first and optimality cuts are generated to update the flow rates. Due to the strong nonconvexity of local subproblems, the GBD may not be able to reach even local optimal solutions. To handle this we use relaxations and restarts. Moreover, proximal terms [40] are involved to enhance the convergence of ADMM-2. The initialization methods are the same as that of the proposed method.

As seen from Fig. 7(a), ADMM-1 performs well in terms of convergence, and the operation cost is higher since flow rates are not optimized. In ADMM-2, although the optimization objective obtain approximately the same results as the proposed method, the results oscillates around the optimal objective value. The oscillations are inferred to mainly result from the bilinear terms in constraint (31), where the fluid flow rates, the flow temperatures and the heating power related to their products are all decision variables. Besides, the primal and dual residuals of fluid flow rates are simultaneously controlled in the optimization process of ADMM-2. Comparatively, the proposed method ensures primal feasibility of fluid flow rates, i.e., the mass conservation in PHN is always guaranteed.

It should also be noted that ADMM-2 is much more time-consuming. For this test case, the total time consumption on a single PC without parallel calculation of the proposed method, ADMM-1 and ADMM-2 is 6min2s, 5min22s, and 2h36min respectively. Considering time delays of communications in application scenarios and larger energy systems, the scalability of both the proposed method and ADMM-1 can be expected. In ADMM-2, the the huge time consumption mainly results from GBD repeatedly solving the subproblems. Although adaptive parameter settings and a stricter selection of the duality gap tolerance may help avoid strong oscillations in ADMM-2, the time consumption can still hinder its applications, and thus we present it as a backup solution to obtain rough results.

D. Impact of Hybrid Quality and Quantity Regulation

To illustrate the effectiveness of the proposed method, we investigate the reference case where fluid flow rates remain history values. The operation status of the DESs is compared in Fig. 8. Some important indices are compared in Table II. It can be observed that with a comprehensive regulation of heat transport through hybrid quality and quantity dispatch, the

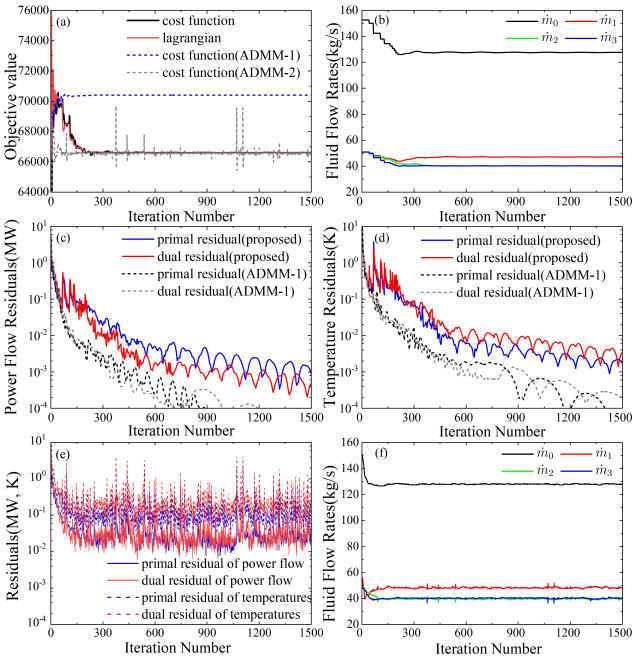

Fig. 7. Convergence trajectories of: (a) Objective function value. (b) Fluid flow rates given by the proposed method. (c) Residuals of transmission line power of the proposed method and ADMM-1. (d) Residuals of PHN flow temperatures of the proposed method and ADMM-1. (e) Residuals of ADMM-2. (f) Fluid flow rates given by ADMM-2.

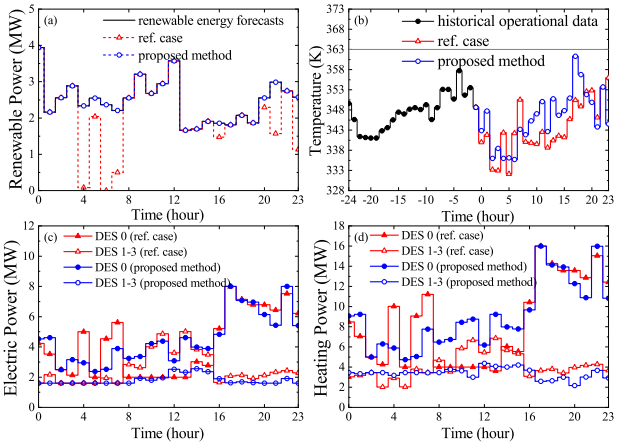

Fig. 8. Operation status of the DESs: (a) Power output of renewable energy sources. (b) Historical and dispatched supply water temperature at HES 0. (c) Electric power output of the CHPs. (d) Heat power output of the CHPs and HPs.

renewable energy is completely accommodated, and the total cost decreases by 5.4%. This is accomplished by decreasing the PHN fluid flow rates by about 5%-20% and appropriately increasing the supply water temperature. The total heat loss is thus reduced.

The improvement in heat losses is subtle and cannot explain the great economic impact of renewable accommodation. Actually, we can note that the DESs serving as HC nodes have lower heat generation and extract more heat from the PHN compared to the reference case, which means the DESs throughout the entire system can work in a more complementary manner. Remembering that in Table I CHP 0 seems expensive in terms of electricity generation but has a higher heat-to-power ratio, increasing its output and decreasing those of CHP 1, 2 and 3 can better make a way for the renewables. The failure of such attempts without fluid flow rates regulation may be explained by the time delay. In the reference case, the pipeline delay time between the DES 0 and the other HC DESs is about 7 hours. If the HC nodes are going to increase heat exchange with the PHN at time section 21 and 23 to provide generation flexibility to the renewables, a certain amount of heat must be stored to the PHN by DES 0 in advance. According to the delay time, appropriate candidate time sections would include time sections 14-16 and 0-5. However, these time sections are load valleys and increasing output of CHP 0 to store the heat may lead to curtailment of the renewables. Another option is to exploit the heat stored in the PHN before the dispatched day. However, as seen from the historical operation data in Fig. 8 (b), the supply water temperature beyond time sections -5-0 is relatively low

TABLE II
COMPARISONS OF THE PROPOSED METHOD AND THE REFERENCE CASE

	Reference Case	Proposed Method
Cost($)	70408.50	66609.88(-5.4%)
Renewable curtailment	17.3%	0.0%
Heat losses(MWh,%)	3.07 (1.03%)	2.06 (0.7%)
$\dot{m}_1$(kg/s)	50.89	47.13
$\dot{m}_2$(kg/s)	50.89	40.21
$\dot{m}_3$(kg/s)	50.89	40.26
Delay time of pipeline 01 (hour)	6	7.15
Delay time of pipeline 12 (hour)	2	2.53
Delay time of pipeline 13 (hour)	2	2.53
Heat injected to the PHN by DES 0 (MWh)	202.47	218.27
Local Heat generation of DES 1, 2, and 3(MWh)	97.88	81.29

and cannot be easily extracted from the PHN. The proposed method increases the average delay time to approximately 9 hours, which enables DES 0 to store heat to the PHN at load peaks and exploit the heat stored before the dispatched day. Therefore, the economy of the connected DESs is significantly increased through a better synergy.

In addition to the delay time, fluid flow rates also relate to the heat capacity flow rates and the thermal resistances of the HESs. Analogic to conventional heat storage devices, the fluid flow rates would affect the heat storage capacities and maximum charging or discharging rates, which are also important but not discussed in detail in the test case. It is obvious that higher fluid flow rates would definitely lead to higher storage capacities and higher maximum charging or discharging rates, and thus benefit the entire system. Yet according to the proposed method, the fluid flow rates should better be decreased, which indicates a dominant effect of delay time in this particular case.

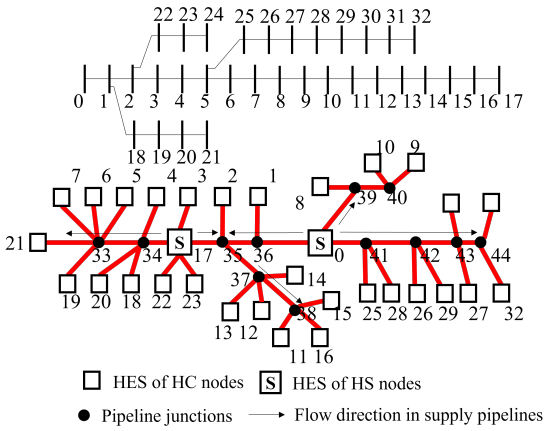

Fig. 9. The topology of the EPN and PHN of the 45-node test system. Nodes with the same labels represent the same DES. Only the supply pipelines are presented and the return pipelines are symmetrical.

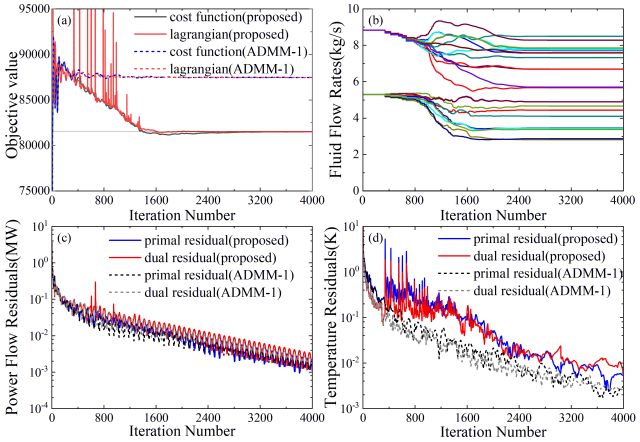

Fig. 10. Convergence trajectories of the proposed method: (a) Objective function value. (b) Fluid flow rates of different HC nodes in the DHN. (c) Residuals of transmission line power. (d) Residuals of PHN flow temperatures.

E. 45-node test system

We further test the proposed method on an larger integrated system, whose topology is shown in Fig. 9. Nodes with the same labels represent the same DES. The pipeline junctions are also treated as DESs and there are in total 45 DESs serving as optimization agents in the system. DES 0 and DES 17 are HS nodes of the PHN. All of the other DESs are equipped with heat pumps and those with high power loads are further equipped with CHPs. The total power load and heat load during the day are 178.3 MWh and 464.7 MWh respectively. The forecast of available renewable sources is 54MWh, among which 34MWh comes from PV panels during the day. The initialization methods and algorithm parameteres are the same as those in the small test system, except that the step size s^{ref} is set to 0.001. More detailed definition of the test system can be found in [30].

Fig. 10 displays the convergence trajectories of the proposed method and ADMM-1. The results of ADMM-2 are not presented due to its time consumption and poor convergence. The decisions of the flow rates tend towards stability after 3000 iterations and the final desicions are quite different from each other and the initial values. It takes about 0.05s for each agent to optimize the subproblem and calculate the gradients. Suppose the time delay in application scenarios is 0.2s, and the total parallel computation time would be about 15min, which is acceptable. As for the proposed method, the objective function may encounter substantial changes due to flow rate variations in the first hundreds of iterations. As the iteration continues, the sharp protuberance disappears and the fluid flow rates are optimized smoothly. Compared to the reference case without flow rate adjustment, the total cost is reduced from 87481.53 to 81512.44(-6.8%) and the curtailment rate of the renewables is reduced from 28.0% to 1.0%. This test case further shows the effectiveness of the proposed method.

V. Conclusion

By applying trigonometric expansion to nodal temperatures, a new model is established to model pipeline dynamics in DHN considering regulation of fluid flow rates. Besides, the heat transfer processes throughout the entire heating system are analyzed and the heat current method is employed to comprehensively model them. On this basis, an optimization model of multiple DESs connected through the EPN and the DHN is established.

To deal with the non-convexity of the model, a primal-decomposition-based decentralized gradient descent method in company with ADMM is proposed to optimize the power and heat transport among multi-agent DESs considering hybrid quality and quantity regulation. The convergence of the optimization approach on the nonconvex model is also discussed.

Case study on two test systems validates the effectiveness of the proposed model and method. The proposed method manages to adjust the fluid flow rates within an acceptable period of time to further harness the flexibility to reduce operation costs in a fully decentralized manner.

Still, the effect of uncertainties are not discussed in this paper. Our future work will further investigate it in the highly integrated user-side energy systems and attempt to propose both a robust day-ahead optimization method and fast on-line adjusting strategies.

References

[1] Q. Wen, G. Liu, Z. Rao, and S. Liao, "Applications, evaluations and supportive strategies of distributed energy systems: A review," *Energy and Buildings*, vol. 225, p. 110314, 2020.

[2] D. K. Molzahn, F. Dörfler, H. Sandberg, S. H. Low, S. Chakrabarti, R. Baldick, and J. Lavaei, "A survey of distributed optimization and control algorithms for electric power systems," *IEEE Transactions on Smart Grid*, vol. 8, no. 6, pp. 2941–2962, 2017.

[3] X. Zheng, Q. Sun, Y. Wang, L. Zheng, X. Gao, S. You, H. Zhang, and K. Shi, "Thermo-hydraulic coupled simulation and analysis of a real large-scale complex district heating network in tianjin," *Energy*, vol. 236, p. 121389, 2021.

[4] X. Qin, H. Sun, X. Shen, Y. Guo, Q. Guo, and T. Xia, "A generalized quasi-dynamic model for electric-heat coupling integrated energy system with distributed energy resources," *Applied Energy*, vol. 251, p. 113270, 2019.

[5] S. Guo, G. Song, M. Li, X. Zhao, Y. He, A. Kurban, W. Ji, and J. Wang, "Multi-objective bi-level quantity regulation scheduling method for electric-thermal integrated energy system considering thermal and hydraulic transient characteristics," *Energy Conversion and Management*, vol. 253, p. 115147, 2022.

[6] B. Rolfsman, "Combined heat-and-power plants and district heating in a deregulated electricity market," *Applied Energy*, vol. 78, no. 1, pp. 37–52, 2004.
[7] X. Chen, C. Kang, M. O'Malley, Q. Xia, J. Bai, C. Liu, R. Sun, W. Wang, and H. Li, "Increasing the flexibility of combined heat and power for wind power integration in china: Modeling and implications," *IEEE Transactions on Power Systems*, vol. 30, no. 4, pp. 1848–1857, 2015.
[8] X. Liu, J. Wu, N. Jenkins, and A. Bagdanavicius, "Combined analysis of electricity and heat networks," *Applied Energy*, vol. 162, pp. 1238–1250, 2016.
[9] D. Xu, Q. Wu, B. Zhou, C. Li, L. Bai, and S. Huang, "Distributed multi-energy operation of coupled electricity, heating, and natural gas networks," *IEEE Transactions on Sustainable Energy*, vol. 11, no. 4, pp. 2457–2469, 2020.
[10] Y. Cao, W. Wei, L. Wu, S. Mei, M. Shahidehpour, and Z. Li, "Decentralized operation of interdependent power distribution network and district heating network: A market-driven approach," *IEEE Transactions on Smart Grid*, vol. 10, no. 5, pp. 5374–5385, 2019.
[11] J. Li, J. Lin, Y. Song, X. Xing, and C. Fu, "Operation optimization of power to hydrogen and heat (p2hh) in adn coordinated with the district heating network," *IEEE Transactions on Sustainable Energy*, vol. 10, no. 4, pp. 1672–1683, 2019.
[12] A. Benonysson, B. Bøhm, and H. F. Ravn, "Operational optimization in a district heating system," *Energy Conversion and Management*, vol. 36, no. 5, pp. 297–314, 1995.
[13] M. Patel, N. Markatos, and M. Cross, "Method of reducing false-diffusion errors in convection—diffusion problems," *Applied Mathematical Modelling*, vol. 9, no. 4, pp. 302–306, 1985.
[14] V. D. Stevanovic, B. Zivkovic, S. Prica, B. Maslovaric, V. Karamarkovic, and V. Trkulja, "Prediction of thermal transients in district heating systems," *Energy Conversion and Management*, vol. 50, no. 9, pp. 2167–2173, 2009.
[15] Y. Chen, Q. Guo, H. Sun, and Z. Pan, "Integrated heat and electricity dispatch for district heating networks with constant mass flow: A generalized phasor method," *IEEE Transactions on Power Systems*, vol. 36, no. 1, pp. 426–437, 2021.
[16] J. Yang, N. Zhang, A. Botterud, and C. Kang, "On an equivalent representation of the dynamics in district heating networks for combined electricity-heat operation," *IEEE Transactions on Power Systems*, vol. 35, no. 1, pp. 560–570, 2020.
[17] Y. Dai, L. Chen, Y. Min, Q. Chen, J. Hao, K. Hu, and F. Xu, "Dispatch model for chp with pipeline and building thermal energy storage considering heat transfer process," *IEEE Transactions on Sustainable Energy*, vol. 10, no. 1, pp. 192–203, 2019.
[18] J. Hao, Q. Chen, K. He, L. Chen, Y. Dai, F. Xu, and Y. Min, "A heat current model for heat transfer/storage systems and its application in integrated analysis and optimization with power systems," *IEEE Trans. Sustain. Energy*, vol. 11, no. 1, pp. 175–184, 2020.
[19] K.-L. He, Q. Chen, H. Ma, T. Zhao, and J.-H. Hao, "An isomorphic multi-energy flow modeling for integrated power and thermal system considering nonlinear heat transfer constraint," *Energy*, vol. 211, p. 119003, 2020.
[20] S. Yao, W. Gu, J. Wu, H. Lu, S. Zhang, Y. Zhou, and S. Lu, "Dynamic energy flow analysis of the heat-electricity integrated energy systems with a novel decomposition-iteration algorithm," *Applied Energy*, vol. 322, p. 119492, 2022.
[21] Y. Xue, Z. Li, C. Lin, Q. Guo, and H. Sun, "Coordinated dispatch of integrated electric and district heating systems using heterogeneous decomposition," *IEEE Transactions on Sustainable Energy*, vol. 11, no. 3, pp. 1495–1507, 2020.
[22] X. Liang, Z. Li, W. Huang, Q. H. Wu, and H. Zhang, "Relaxed alternating direction method of multipliers for hedging communication packet loss in integrated electrical and heating system," *Journal of Modern Power Systems and Clean Energy*, vol. 8, no. 5, pp. 874–883, 2020.
[23] J. Huang, Z. Li, and Q. Wu, "Coordinated dispatch of electric power and district heating networks: A decentralized solution using optimality condition decomposition," *Applied Energy*, vol. 206, pp. 1508–1522, 2017.
[24] Z. G. Li, W. C. Wu, J. H. Wang, B. M. Zhang, and T. Y. Zheng, "Transmission-constrained unit commitment considering combined electricity and district heating networks," *Ieee Transactions on Sustainable Energy*, vol. 7, no. 2, pp. 480–492, 2016.
[25] Z. Yifan, H. Wei, Z. Le, M. Yong, C. Lei, L. Zongxiang, and D. Ling, "Power and energy flexibility of district heating system and its application in wide-area power and heat dispatch," *Energy*, vol. 190, p. 116426, 2020.
[26] Z. Li, W. Wu, M. Shahidehpour, J. Wang, and B. Zhang, "Combined heat and power dispatch considering pipeline energy storage of district heating network," *IEEE Transactions on Sustainable Energy*, vol. 7, no. 1, pp. 12–22, 2016.
[27] Y. Jiang, C. Wan, A. Botterud, Y. Song, and S. Xia, "Exploiting flexibility of district heating networks in combined heat and power dispatch," *IEEE Transactions on Sustainable Energy*, vol. 11, no. 4, pp. 2174–2188, 2020.
[28] Q. Sun, Q. Chen, and K. He, "Fully decentralized dispatch of integrated power distribution and heating systems considering nonlinear heat transfer processes," in *2022 IEEE Power and Energy Society General Meeting (PESGM)*, 2022, to appear in.
[29] H. Zhao, "Analysis, modelling and operational optimization of district heating systems," Ph.D. dissertation, Danmarks Tekniske Univ., Aug 1995.
[30] "Supplementary Materials for Decentralized Dispatch with Comprehensive Regulation of Heat Transport in DHN." [Online]. Available: https://github.com/falcon-sqh/TSTE-dec_dispatch_EPN_DHN
[31] M. E. Baran and F. F. Wu, "Optimal capacitor placement on radial distribution systems," *IEEE Transactions on Power Delivery*, vol. 4, no. 1, pp. 725–734, 1989.
[32] M. Farivar and S. H. Low, "Branch flow model: Relaxations and convexification—part i," *IEEE Transactions on Power Systems*, vol. 28, no. 3, pp. 2554–2564, 2013.
[33] Z. Yang, R. Wu, J. Yang, K. Long, and P. You, "Economical operation of microgrid with various devices via distributed optimization," *IEEE Trans. Smart Grid*, vol. 7, no. 2, pp. 857–867, 2016.
[34] S. Boyd, N. Parikh, E. Chu, B. Peleato, and J. Eckstein, *Distributed Optimization and Statistical Learning via the Alternating Direction Method of Multipliers*. Now Publishers Inc., 2011.
[35] A. Rabiee, B. Mohammadi-Ivatloo, and M. Moradi-Dalvand, "Fast dynamic economic power dispatch problems solution via optimality condition decomposition," *IEEE Trans. Power Syst.*, vol. 29, no. 2, pp. 982–983, 2014.
[36] O. Gannot, "A frequency-domain analysis of inexact gradient methods," *Mathematical Programming*, pp. 1–42, 2021.
[37] S. Mhanna, G. Verbič, and A. C. Chapman, "Adaptive admm for distributed ac optimal power flow," *IEEE Transactions on Power Systems*, vol. 34, no. 3, pp. 2025–2035, 2019.
[38] A. Domahidi, E. Chu, and S. Boyd, "Ecos: An socp solver for embedded systems," in *2013 European Control Conference (ECC)*, 2013, pp. 3071–3076.
[39] A. M. Geoffrion, "Generalized benders decomposition," *Journal of Optimization Theory and Applications*, vol. 10, no. 4, pp. 237–260, 1972.
[40] M. Ma, L. Fan, and Z. Miao, "Consensus admm and proximal admm for economic dispatch and ac opf with socp relaxation," in *2016 North American Power Symposium (NAPS)*, 2016, pp. 1–6.

Qinghan Sun (S'22) was born in China in 1998. He received the B.Sc. degree in Advanced Clean Energy(ACE) Program from Tsinghua University, Beijing, China, in 2020. He is now a Ph.D candidate in the Department of Engineering Mechanics, Tsinghua University. His current interests include user-side multi-energy systems.

Tian Zhao was born in China in 1992. He received the B.Sc. degree (2013) and the Ph.D. degree (2019) in engineering thermophysics from Tsinghua University in China. He is now a postdoctoral researcher in Department of Engineering Mechanics, Tsinghua University. His current interests include integrated power and thermal energy systems and energy storage.

Qun Chen (M'16) was born in China in 1981. He received the B.Sc. degree (2003) and the Ph.D. degree (2008) in engineering thermophysics from Xi'an Jiaotong University and Tsinghua University, respectively, in China. He is now a professor, Department of Engineering Mechanics, Tsinghua University. His current interests include integrated power and thermal energy systems and micro energy systems

Kelun He was born in China in 1993. He received the B.Sc. degree (2015) and the Ph.D. degree (2021) in engineering thermophysics from Tsinghua University, in China. He is now a postdoctoral researcher in Department of Engineering Mechanics, Tsinghua University. His current interests include integrated power and thermal energy systems modelling and control.

Huan Ma was born in China in 1995. He received the B.Sc. degree and the Ph.D. degree from Tsinghua University, Beijing, China, in 2017 and 2022, respectively. He is now a Post-Doc Researcher in the Department of Engineering Mechanics, Tsinghua University. His research interests are in modelling and analysis of the integrated power and thermal systems.